Homotopy Solution for Non-Similarity Boundary-Layer Flow near a Stagnation Point

Xiangcheng You and Hang Xu

State Key Lab of Ocean Engineering, School of Naval Architecture, Ocean and Civil Engineering, Shanghai Jiao Tong University, Shanghai 200240, China

Reprint requests to X. Y.; E-mail: xcyou@sjtu.edu.cn

In this paper, non-similarity boundary-layer flow of a Newtonian fluid near an asymmetric plane stagnation point with a dimensionless external flow velocity $u_e = x/(x+1)$ is studied. The original boundary-layer equations are transferred into a nonlinear partial differential equation (PDE) with variable coefficients. An analytic technique for strongly nonlinear equations, namely the homotopy analysis method (HAM), is applied to replace the nonlinear PDE by an infinite number of linear ordinary differential equations (ODEs) with constant coefficients. An artificial parameter, called the convergence-control parameter, is introduced to ensure the convergence of solution series. Accurate analytical approximations of skin friction and boundary-layer thickness are obtained, and the effect of the external flow velocity on the non-similarity flows is investigated. This approach has general meanings and can be applied to many other non-similarity boundary-layer flows.

Key words: Non-Similarity; Boundary-Layer; Stagnation Point Flow; Series Solution.

1. Introduction

Stagnation point flows are often occurred in science and engineering. In some situations, flows can be viscous or inviscid, steady or unsteady, two or three-dimensional, normal or oblique, and forward or reverse. Hiemenz [1] studied the two-dimensional axisymmetric flows, and Homann [2] investigated the three-dimensional stagnation point flows. These are exact solutions of the Navier-Stokes equations in certain particular cases in which the flows are directed perpendicular to an infinite flat plate or an infinite circular cylinder. Hadamard [3] solved the forward and reverse two-fluid stagnation point flows with limited Reynolds number. Howarth [4] and Davey [5] presented results for unsymmetric cases of three-dimensional stagnation point flows. Wang [6] obtained an exact solution for the axisymmetric stagnation flow on a circular cylinder. Tilley and Weidman [7] gave the exact similarity solutions for the steady impingement of two viscous, immiscible oblique stagnation flows forming a plane interface. Pop [8], Lawrence and Rao [9] investigated the effects of magnetic field on a steady boundary-layer flow of an incompressible viscous fluid near an asymmetric plane stagnation point. All of these works enrich our understandings about stagnation point boundary-layer flows. It

is known that most of boundary-layer problems are resolved based on the similarity solutions [10 – 14]. However, most boundary-layer flows in nature are not similarity ones. Unlike similarity boundary-layer flows that are governed by nonlinear ODEs, non-similarity flows are governed by nonlinear PDEs. Mathematically, it is much more difficult to solve a PDE than an ODE. This is the reason why most publications about boundary-layer flows are related to similarity flows.

As mentioned by Sparrow and Quack [15], non-similarity of boundary-layer flows may be caused by many reasons, such as spatial variations in free stream velocity, sheet mass transfer, transverse curvature, and so on. For similarity boundary-layer flows, all velocity profiles across the flow direction are similar by means of a similarity-variable. However, such kind of similarity is lost for non-similarity flows [16 – 20], and they only exist as special cases. However, physically speaking, non-similarity boundary-layer flows are more general, and thus are more important than similarity ones. Due to its complexity, very limited attempt has been made in solving non-similarity flows. It is a pity that much less attentions have been paid to non-similarity flows. In this paper, we provide here a general analytic approach for non-similarity boundary-layer flows, by introducing a set of global non-similarity variables, the original boundary-layer equations are transformed into
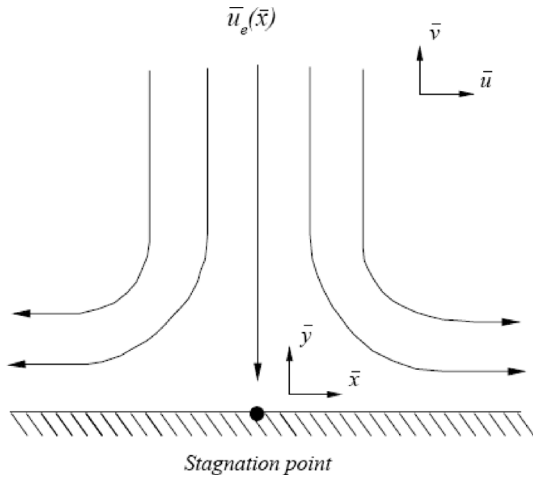
$$\bar{u}_e(\bar{x})$$

Fig. 1. Physical model and coordinate system.

a nonlinear partial differential equation with variable coefficients.

Without loss of generality, let us consider a steady asymmetric boundary-layer flow of a Newtonian fluid near a plane stagnation point with the external flow velocity $\bar{u}_e = U_0\bar{x}/(\bar{x}+L_0)$ in the upper quarter plane $\bar{x} \geq 0$ and $\bar{y} \geq 0$, where the $\bar{x}$-axis is along the wall and the $\bar{y}$-axis normal to it, $U_0 > 0$ and $L_0 > 0$ are reference velocity and length, respectively. The flow configuration is shown schematically in Figure 1, together with the corresponding Cartesian coordinates in the horizontal and vertical directions. For more details about its physical background, readers are referred to references [21 – 24]. In the framework of the boundary-layer theory, the steady two-dimensional boundary-layer flow of a Newtonian fluid is governed by

$$\frac{\partial \bar{u}}{\partial \bar{x}} + \frac{\partial \bar{v}}{\partial \bar{y}} = 0, \tag{1}$$

$$\bar{u}\frac{\partial \bar{u}}{\partial \bar{x}} + \bar{v}\frac{\partial \bar{u}}{\partial \bar{y}} = \nu\frac{\partial^2 \bar{u}}{\partial \bar{y}^2} + \bar{u}_e\frac{d\bar{u}_e}{d\bar{x}}, \tag{2}$$

subject to the boundary conditions

$$\bar{y} = 0, \quad \bar{u} = 0, \quad \bar{v} = 0, \tag{3}$$

$$\bar{y} \to +\infty, \quad \bar{u} = \bar{u}_e = \frac{U_0\bar{x}}{(\bar{x}+L_0)}, \tag{4}$$

where $(\bar{u},\bar{v})$ denotes the velocity components, ν the kinematic viscosity of the fluid, respectively.

Introducing the non-dimensional quantities

$$x = \frac{\bar{x}}{L_0}, \quad y = \mathrm{Re}^{1/2}\frac{\bar{y}}{L_0}, \quad u = \frac{\bar{u}}{U_0},$$
$$v = \mathrm{Re}^{1/2}\frac{\bar{v}}{U_0}, \tag{5}$$

where the Reynolds number $\mathrm{Re} = U_0L_0/\nu$ is formed with the reference velocity U_0 and the reference length L_0. Substituting (5) into (1) – (2), we obtain the dimensionless governing equations

$$\frac{\partial u}{\partial x} + \frac{\partial v}{\partial y} = 0, \tag{6}$$

$$u\frac{\partial u}{\partial x} + v\frac{\partial u}{\partial y} = \frac{\partial^2 u}{\partial y^2} + u_e\frac{du_e}{dx}, \tag{7}$$

subject to the boundary conditions

$$y = 0, \quad u = 0, \quad v = 0, \tag{8}$$

$$y \to +\infty, \quad y = u_e(x) = \frac{x}{(x+1)}. \tag{9}$$

The continuity equation (6) is automatically satisfied by defining a stream function $\psi(x,y)$ such that

$$u = \frac{\partial \psi}{\partial y}, \quad v = -\frac{\partial \psi}{\partial x}. \tag{10}$$

It is well known that, when the external flow velocity is in the form $u_e(x) = Ax^\lambda$ with a constant A, there exist the similarity boundary-layer flows with the similarity-variables

$$\psi = Ax^{(\lambda+1)/2}\hat{f}(\eta), \quad \eta = yx^{(\lambda-1)/2},$$

and the original PDEs can be replaced by a nonlinear ODE about $\hat{f}(\eta)$. Especially, the similarity variable is $\eta = y$ when $u_e(x) = x$, and $\eta = y/\sqrt{x}$ when $u_e(x) = 1$, respectively. However, with the external flow velocity $u_e = x/(1+x)$, the corresponding boundary-layer flow is of non-similarity. Therefore, it is impossible to rewrite the original partial differential equations (PDEs) in an ordinary differential equation (ODE). For the non-similarity boundary-layer flow, a more general transformation

$$\psi = \sigma(x)f(x,\eta), \quad \eta = \frac{y}{\sigma(x)} \tag{11}$$

should be used, where $\sigma(x) > 0$ is a real function to be determined later. Note that the above-mentioned similarity variable $\eta = yx^{(\lambda-1)/2}$ can be regarded as a special case of $\eta = y/\sigma(x)$. Then, we have

$$
\begin{aligned}
u &= \frac{\partial \psi}{\partial y} = \frac{\partial f}{\partial \eta}, \\
v &= -\frac{\partial \psi}{\partial x} = \sigma'(x)\left(\eta\frac{\partial f}{\partial \eta} - f\right) - \sigma(x)\frac{\partial f}{\partial x},
\end{aligned}
\tag{12}
$$

and the governing equation becomes

$$
\begin{aligned}
&\frac{\partial^3 f}{\partial \eta^3} + \frac{1}{2}[\sigma^2(x)]'f\frac{\partial^2 f}{\partial \eta^2} = \\
&\sigma^2(s)\left(\frac{\partial f}{\partial \eta}\frac{\partial^2 f}{\partial x\partial \eta} - \frac{\partial f}{\partial x}\frac{\partial^2 f}{\partial \eta^2}\right) - \sigma^2(x)u_e\frac{du_e}{dx},
\end{aligned}
\tag{13}
$$

subject to the boundary conditions

$$
\begin{aligned}
&f(x,0) = 0, \quad f_\eta(x,0) = 0, \\
&f_\eta(x,+\infty) = u_e(x) = x/(1+x),
\end{aligned}
\tag{14}
$$

where f_η denotes the partial derivative with respect to η.

Let us consider the external flow velocity $u_e(x) = x/(x+1)$. Note that $u_e \to x$ as $x \to 0$, and $u_e \to 1$ as $x \to +\infty$, respectively. Thus, physically, the non-similarity flow near $x = 0$ should be close to the similarity ones corresponding to the external flow velocity $u_e = x$ with the similarity variable y. In addition, and besides, the non-similarity flow as $x \to +\infty$ should be close (but might be *not* equal) to the similarity ones corresponding to the external flow velocity $u_e = 1$ with the similarity variable $y/\sqrt{x}$ as $x \to +\infty$. Therefore, according to the definition (11) of the variable $\eta = y/\sigma(x)$ for the non-similarity flow, it is natural for us to choose

$$
\sigma(x) = \sqrt{x+1},
\tag{15}
$$

so that η tends to y as $x \to 0$, and to $y/\sqrt{x}$ as $x \to +\infty$, respectively. Besides, according to the expressions of the external flow velocity $u_e = x/(1+x)$ and $\sigma(x) = \sqrt{1+x}$, it is natural to define such a new variable

$$
\xi = \frac{x}{x+1}.
\tag{16}
$$

Then, the governing equation (13) becomes

$$
\begin{aligned}
&\frac{\partial^3 f}{\partial \eta^3} + \frac{1}{2}f\frac{\partial^2 f}{\partial \eta^2} = \\
&(1-\xi)\left(\frac{\partial f}{\partial \eta}\frac{\partial^2 f}{\partial \xi\partial \eta} - \frac{\partial f}{\partial \xi}\frac{\partial^2 f}{\partial \eta^2}\right) - \xi(1-\xi),
\end{aligned}
\tag{17}
$$

subject to the boundary conditions

$$
f(\xi,0) = 0, \quad f_\eta(\xi,0) = 0, \quad f_\eta(\xi,+\infty) = \xi.
\tag{18}
$$

Mathematically, this kind of *nonlinear* PDE with *variable* coefficients is hard to solve, especially by means of analytic methods. This is the main reason why most publications of boundary-layer flows are related to similarity flows governed by ODEs.

Currently, an analytic technique, called the homotopy analysis method (HAM) [25 – 28], has been widely applied to solve nonlinear problems. Different from perturbation techniques, the HAM does not depend upon any small/large physical parameters. More importantly, unlike all other traditional analytic techniques, it provides a convenient way to ensure the convergence of solution series. Thus, the HAM is valid for different types of strongly nonlinear problems in science and engineering [29 – 39]. For example, by means of the HAM, Liao [29] gave a series solution for the similarity Blasius boundary-layer flows, which is convergent in the whole physical domain for all physical parameters. Besides, Liao and Magyari [30] applied the HAM to find some new algebraically decaying boundary-layer flows, which have been never reported and even have been neglected by numerical methods. Furthermore, Abbasbandy [31] applied the HAM to investigate a nonlinear heat transfer problem. Zhu [32] applied the HAM to give, for the first time, an analytic expression for American put option in finance. By means of the HAM, Yamashita et al. [33] obtained a convergent time series for projectile motion. Wu and Cheung [34] applied the HAM to develop an explicit numerical approach for Riemman problems. Recently, they [35] introduced a new auxiliary parameter into the homotopy function and the convergence rate of the series solution is improved. All of these indicate the potential of the HAM as a powerful research tool. Currently, the HAM has been successfully applied to solve some nonlinear PDEs, such as the two-dimensional Gelfand equation [36], the unsteady three-dimensional similarity boundary-layer flows [37], nonlinear progressive waves in water of finite depth [38], the interaction of water wave and non-uniform currents [39], and so on. In this manuscript, we further apply the HAM to solve the non-similarity flow governed by the nonlinear PDEs (17) and (18), and reveal some physical properties of the non-similarity flow.

2. Mathematical Formulations

Mathematically, unlike perturbation techniques and other traditional analytic methods, the HAM provides us great freedom to choose better base functions so as to approximate solutions of nonlinear problems more effectively [29 – 34, 36 – 39]. Physically, it is well known that, in most cases, boundary-layer flows decay exponentially as $\eta \to +\infty$ (for examples, please refer to [29, 37, 40]). Besides, ξ explicitly appears in the governing equation (17) and the boundary condition (18). Therefore, without solving (17) and (18), it is clear that $f(\xi, \eta)$ can be expressed by the following set of base functions

$$\{\xi^k \eta^m \exp(-n\gamma\eta) | k \geq 0, \quad m \geq 0, \quad n \geq 0\} \quad (19)$$

such that

$$f(\xi, \eta) = \sum_{k=0}^{+\infty} \sum_{m=0}^{+\infty} \sum_{n=0}^{+\infty} a_k^{m,n} \xi^k \eta^m \exp(-n\gamma\eta), \quad (20)$$

where $\gamma > 0$ is an auxiliary parameter to be determined later, called the spatial parameter, $a_k^{m,n}$ is a coefficient independent of ξ and η, respectively. This provides us the so-called *solution expression* of $f(\xi, \eta)$: our goal is to give a convergent series solution expressed in the above form.

Based on the governing equation (17), we define a nonlinear operator

$$\mathcal{N}[F(\xi, \eta; q)] = \frac{\partial^3 F}{\partial \eta^3} + \frac{1}{2} F \frac{\partial^2 F}{\partial \eta^2}$$
$$\hspace{2cm} (21)$$
$$- (1 - \xi) \left(\frac{\partial F}{\partial \eta} \frac{\partial^2 F}{\partial \xi \partial \eta} - \frac{\partial F}{\partial \xi} \frac{\partial^2 F}{\partial \eta^2} \right) + \xi(1 - \xi),$$

where $q \in [0, 1]$ is an embedding parameter, $F(\xi, \eta; p)$ is a mapping of $f(\xi, \eta)$, respectively. Let L denote an auxiliary linear operator, $\hbar$ an auxiliary non-zero parameter (called convergence-control parameter), $f_0(\xi, \eta)$ an initial guess of $f(\xi, \eta)$ which satisfies the boundary conditions (18). Now we construct the so-called zeroth-order deformation equation

$$(1 - q)\mathcal{L}[|F(\xi, \eta; q) - f_0(\xi, \eta)] = q\hbar\mathcal{N}[F(\xi, \eta; q)], \quad (22)$$

subject to the boundary conditions

$$F(\xi, 0; q) = 0, \quad \left. \frac{\partial F(\xi, \eta; q)}{\partial \eta} \right|_{\eta=0} = 0,$$
$$\left. \frac{\partial F(\xi, \eta; q)}{\partial \eta} \right|_{\eta \to +\infty} = \xi. \quad (23)$$

Obviously, when $q = 0$ and $q = 1$, we have

$$F(\xi, \eta; 0) = f_0(\xi, \eta), \quad F(\xi, \eta; 1) = f(\xi, \eta), \quad (24)$$

respectively. Note that we have great freedom to choose L, $\hbar$, and $f_0(\xi, \eta)$. So it is reasonable to assume that L, $\hbar$, and $f_0(\xi, \eta)$ are so properly chosen that the above equation has at least one solution $F(\xi, \eta; q)$ in $q \in [0, 1]$, and besides $F(\xi, \eta; q)$ is *continuous* enough with respect to $q \in [0, 1]$. Therefore, as q increases from 0 to 1, $F(\xi, \eta; q)$ varies *continuously* from the initial guess $f_0(\xi, \eta)$ to the exact solution $f(\xi, \eta)$ of (17) – (18). Then, by Taylor's theorem, we can expand $F(\xi, \eta; q)$ in the power series

$$f(\xi, \eta) = F(\xi, \eta; 0) + \sum_{n=1}^{+\infty} f_n(\xi, \eta)q^n, \quad (25)$$

where

$$f_n(\xi, \eta) = \frac{1}{n!} \left. \frac{\partial^n F(\xi, \eta; q)}{\partial q^n} \right|_{q=0}. \quad (26)$$

As mentioned before, we have great freedom to choose the auxiliary linear operator L, the initial guess $f_0(\xi, \eta)$, and the convergence-control parameter $\hbar$. Assuming that L, $f_0(\xi, \eta)$, and $\hbar$ are properly chosen so that the series (25) converges at $q = 1$, we have, from (24), the series solution

$$f(\xi, \eta) = f_0(\xi, \eta) + \sum_{m=1}^{+\infty} f_m(\xi, \eta). \quad (27)$$

According to the fundamental theorem in calculus, the coefficients of Taylor series of a function are unique. Thus, the governing equations and boundary conditions of $f_m(\xi, \eta)$ are unique, and are completely determined by the zeroth-order deformation equations (22) and (23). So, one can obtain the same equations and boundary conditions of $f_m(\xi, \eta)$ by different ways. For example, the governing equations and boundary conditions of $f_m(\xi, \eta)$ can be obtained by means of "the method of Frobenius" [41]: substituting the series (25) into the zeroth-order deformation equations (22) and (23), then equating the coefficients of the like-power of q, one has the mth-order deformation equations

$$\mathcal{L}[f_m(\xi, \eta) - \chi_m f_{m-1}(\xi, \eta)] = \hbar R_m(\xi, \eta), \, m \geq 1, \, (28)$$

subject to the boundary conditions

$$f_m(\xi,0) = 0, \quad \left.\frac{\partial f_m(\xi,\eta)}{\partial\eta}\right|_{\eta=0} = 0,$$
$$\left.\frac{\partial f_m(\xi,\eta;q)}{\partial\eta}\right|_{\eta\to+\infty} = 0, \quad (29)$$

where

$$R_m(\xi,\eta) = \frac{\partial^3 f_{m-1}}{\partial\eta^3} \frac{1}{2} \sum_{n=1}^{m-1} f_{m-1-n} \frac{\partial^2 f_n}{\partial\eta^2}$$
$$-(1-\xi)\sum_{n=1}^{m-1}\left(\frac{\partial f_n}{\partial\eta}\frac{\partial^2 f_{m-1-n}}{\partial\xi\partial\eta} - \frac{\partial f_n}{\partial\xi}\frac{\partial^2 f_{m-1-n}}{\partial\eta^2}\right) \quad (30)$$
$$+(1-\chi_m)\xi(1-\xi),$$

and

$$\chi_m = \begin{cases} 1, & m > 1, \\ 0, & m = 1. \end{cases} \quad (31)$$

Note that Liao [26] provided a rather general approach to get the high-order deformation equations. Using Liao's approach, one can get exactly the same governing equations and boundary conditions of $f_m(\xi,\eta)$ as above. For details, please refer to Liao and Tan [36].

The auxiliary linear operator L and the initial guess $f_0(\xi,\eta)$ should be chosen in such a way that the high-order deformation equations (28) and (29) always have solutions, while the solution expression (20) is satisfied. First, considering the *solution expression* (20) and using the boundary conditions (18), it is straightforward to choose the initial guess

$$f_0(\xi,\eta) = u_e(\xi)\left(\eta - \frac{1-e^{-\gamma\eta}}{\gamma}\right)$$
$$= \xi\left(\eta - \frac{1-e^{\gamma\eta}}{\gamma}\right). \quad (32)$$

Secondly, it is physically well known that the velocity variation across the flow direction is much larger than that in the flow direction. So, physically speaking, the derivative with respect to η is much greater than that with respect to ξ. Keeping this in mind and considering the solution expression (20) and the solution existence of $(28)-(29)$, we choose such an auxiliary linear operator

$$\mathcal{L}[F] = \frac{\partial^3 F}{\partial\eta^3} + \gamma\frac{\partial^2 F}{\partial\eta^2}, \quad (33)$$

with the property

$$\mathcal{L}[C_0 + C_1\exp(-\gamma\eta) + C_2\eta] = 0, \quad (34)$$

where C_0, C_1, and C_2 are integral coefficients independent of η. For details of the choice of the auxiliary linear operator, please refer to Tan and Liao [37].

Note that the right-hand side of (28) is known, and its left-hand side is *independent* of ξ. Thus, (28) is in fact an *ordinary* differential equation (ODE) with respect to η, and therefore is easy to solve! The particular solution of (28) reads

$$f_m^*(\xi,\eta) = \chi_m f_{m-1}(\xi,\eta)$$
$$+ \hbar\int^\eta\left\{\int^\eta\left[e^{-\gamma\eta}\int^\eta R_m(\xi,s)e^{\gamma s}ds\right]d\eta\right\}d\eta. \quad (35)$$

According to (34), its general solution reads

$$f_m(\xi,\eta) = f_m^*(\xi,\eta) + C_{0,m}$$
$$+ C_{1,m}\exp(-\gamma\eta) + C_{2,m}\exp(+\gamma\eta), \quad (36)$$

where the three integral coefficients

$$C_{0,m} = -f_m^*(\xi,0) - \frac{1}{\gamma}\frac{\partial f_m^*}{\partial\eta}, \quad C_{1,m} = -\frac{1}{\gamma}\frac{\partial f_m^*}{\partial\eta},$$
$$C_{2,m} = 0 \quad (37)$$

are uniformly determined by the boundary conditions (29). In this way, it is rather easy to solve the linear equations (28) and (29) successively, especially by means of the symbolic computation software such as Maple, Mathematica, and so on.

In this way, the original *nonlinear* PDE (17) with *variable* coefficients is transferred into an infinite number of *linear* ODEs (28) with *constant* coefficients. Obviously, a linear ODE with constant coefficient is much easier to solve than a nonlinear PDE with variable coefficients. Note that, different from perturbation techniques, such kind of transformation does not need any small physical parameters. Besides, it should be emphasized that the chosen auxiliary linear operator (33) has not an obvious relationship with the linear term $f_{\eta\eta\eta}$ in the original equation (17). This is mainly because, unlike all of other analytic techniques, the homotopy analysis method provides us with great freedom to choose the auxiliary linear operator. Without such kind of freedom, it is impossible for us to transfer the original nonlinear PDE (17) with variable coefficients into the linear ODEs (28) with constant coefficients.

It should be emphasized that some similarity boundary-layer flows are solved by means of the HAM using the *same* auxiliary linear operator (33) and the rather similar initial guess. For example, Liao [29] used the *same* auxiliary operator (33) to solve the *similarity* Blasius boundary-layer flows. Note that the auxiliary linear operator (33) contains only derivatives with respect to η, although the nonlinear PDE (17) contains derivatives with respect to both η and ξ. Mathematically, this is because the HAM provides us great freedom to choose the auxiliary linear operator, and more importantly, it also provides a convenient way to ensure the convergence of solution series. Physically, this is due to the existence of the boundary layer: the velocity variation across the flow direction (denoted by η) is much larger than that in the flow direction (denoted by ξ). Therefore, by means of HAM, one can solve non-similarity flows in the same way as similarity ones: only more CPU time is needed. So, by means of the HAM, it is *not* more difficult to solve non-similarity boundary-layer flows than similarity ones.

3. Results Analysis

3.1. Convergence of Solution Series

Unlike all other analytic techniques, the HAM provides a convenient way to ensure the convergence of solution series, as shown in [29 – 34, 36 – 39]. Note that the solution series (27) contains the so-called convergence-control parameter $\hbar$ and the spatial-scale parameter γ, which have no physical meanings but can be used to ensure the convergence of the solution series. Obviously, if the solution series (27) is convergent, the corresponding 2nd-order derivative $f_{\eta\eta}(\xi,\eta)$ should converge, too. For simplicity, let us consider the convergence of the series of $f_{\eta\eta}(\xi,0)$, which is dependent on the two auxiliary parameters $\hbar$ and γ but has clear physical meanings. First of all, set $\hbar = -1$ and regard γ as an unknown variable. It is found that the series of $f_{\eta\eta}(\xi,0)$ converges to the same value for large enough value of γ ($\gamma \geq 4$), as shown in Figure 2. Thus, we simply take $\gamma = 4$. Then, $f_{\eta\eta}(\xi,0)$ is dependent on both the physical variable ξ and the convergence-control parameter $\hbar$. So, from mathematical view points, given a value of ξ, $f_{\eta\eta}(\xi,0)$ is a power series of $\hbar$ and thus its convergence is determined by $\hbar$. Thus, regarding $\hbar$ as a variable, we can plot the curves of $f_{\eta\eta}(\xi,0) \sim \hbar$ for different values of ξ varying from 0 to 1, as shown in Figure 3. Physi-
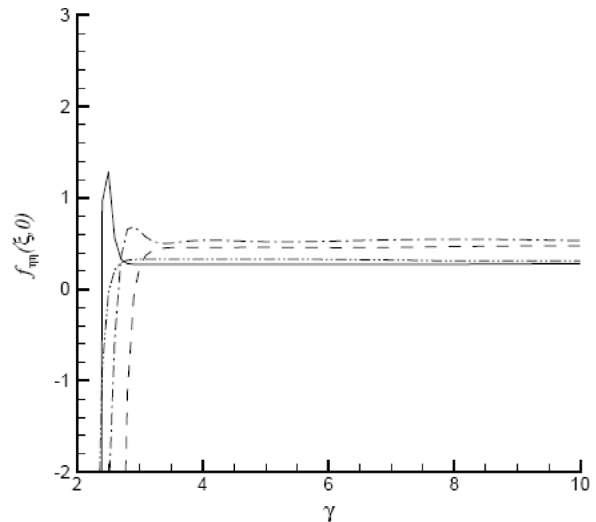

Fig. 2. Curves $f_{\eta\eta}(\xi,0) \sim \gamma$ at the 15th-order approximation given by $\hbar = -1$; Solid line: $\xi = 1/4$; Dashed line: $\xi = 1/2$; Dash-dotted line: $\xi = 3/4$; Dash-dot-dotted line: $\xi = 1$.
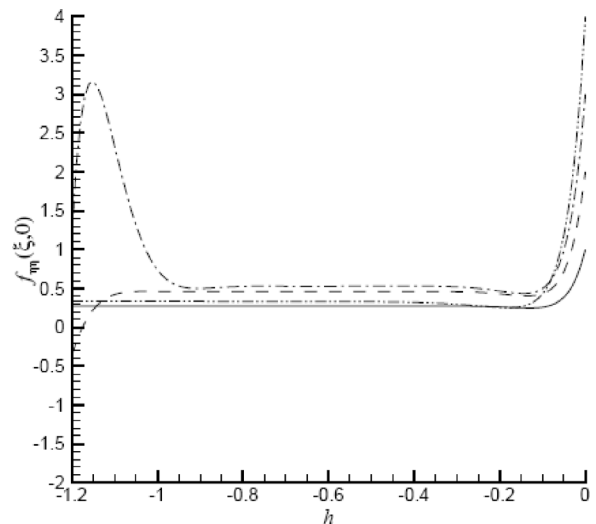

Fig. 3. Curves $f_{\eta\eta}(\xi,0) \sim \hbar$ at the 25th-order approximation given by $\gamma = 4$; Solid line: $\xi = 1/4$; Dashed line: $\xi = 1/2$; Dash-dotted line: $\xi = 3/4$; Dash-dot-dotted line: $\xi = 1$.

cally, for given ξ, $f_{\eta\eta}(\xi,0)$ is independent of both $\hbar$ and λ. Note that for any given value of $\xi \in [0,1]$ $f_{\eta\eta}(\xi,0)$ converges to the same value in the case of $\hbar \in [-3/5, -1/10]$. Thus, as long as we choose a value of $\hbar$ in the region $-3/5 \leq h \leq -1/10$, we can get a convergent series solution of $f_{\eta\eta}(\xi,0)$ in the whole region $\xi \in [0,1]$. So, in this paper we use $\hbar = -3/5$ and $\gamma = 4$ to get a convergence series solution for the non-similarity flow. It should be emphasized that, when
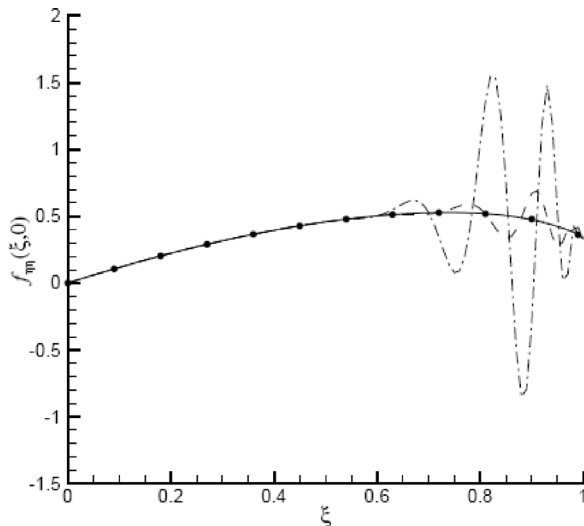
Fig. 4. Curves $f_{\eta\eta}(\xi,0) \sim \xi$ by means of $\gamma = 4$ but different values of $\hbar$. Solid line: 30th-order approximation when $\hbar = -3/5$; Symbols: 35th-order approximation when $\hbar - 3/5$; Dash-dotted line: 30th-order approximation when $\hbar = -9/10$; Dash-dot-dotted line: 30th-order approximation when $\hbar = -1$.

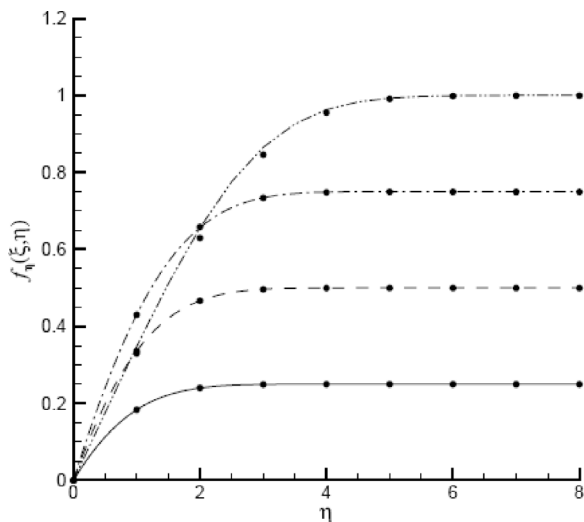Fig. 5. Velocity profiles $f_{\eta}(\xi,0)$ given by $\gamma = 4$ and $\hbar = -3/5$; Solid line: $\xi = 1/4$; Dashed line: $\xi = 1/2$; Dash-dotted line: $\xi = 3/4$; Dash-dot-dotted line: $\xi = 1$; Symbols: numerical results.

$\hbar \notin [-3/5, -1/10]$ such as $\hbar = -9/10$ or $\hbar = -1$, the series solution of $f_{\eta\eta}(\xi,0)$ converges only for small ξ and $\xi = 1$, corresponding to small x and $x \to +\infty$, respectively, but diverges for some values of ξ, as shown in Figure 4. Furthermore, it is found that as long as the series of $f_{\eta\eta}(\xi,0)$ is convergent in the region $\xi \in [0,1]$

the corresponding series of $f(\xi,\eta)$, $f_{\eta}(\xi,\eta)$, and so on, are also convergent in the whole region $0 \leq \xi \leq 1$ and $0 \leq \eta < +\infty$, corresponding to $0 \leq x < +\infty$ and $0 \leq y < +\infty$. To illustrate the convergence of the solution series (25), we compare the convergent series solution with numerical results given by the Keller-Box method [42], and very good agreement is found, as shown in Figure 5. So, it is very important to choose a proper value of the convergence-control parameter $\hbar$, and plotting curves like $f_{\eta\eta}(\xi,0) \sim \hbar$ indeed provides us a convenient way to do so. For details of choosing the convergence-control parameter $\hbar$, please refer to Liao and Tan [36, 37].

Note that $\hbar = -3/5$ and $\gamma = 4$ are not the optimal values that should be determined by minimizing the integral of the square residual error of the governing equation over the whole domain $0 \leq \xi \leq 1$ and $0 \leq \eta < +\infty$. However, these values are good enough to get a convergence series solution of the non-similarity flow. All conclusions given in the following two subsections are based on this convergent series solution.

3.2. Boundary-Layer Thickness

It is well known that there exists the similarity boundary-layer flow when the external flow velocity $u_e = 1$ with the similarity variable $\eta = y/\sqrt{x}$. Besides, the considered external flow velocity $u_e = x/(1+x)$ tends to 1 as $x \to +\infty$, as shown in Figure 6. Then, one question arises: are the boundary-layer thickness and the local skin friction coefficient of the non-similarity flow different from those of similarity ones as $x \to +\infty$?
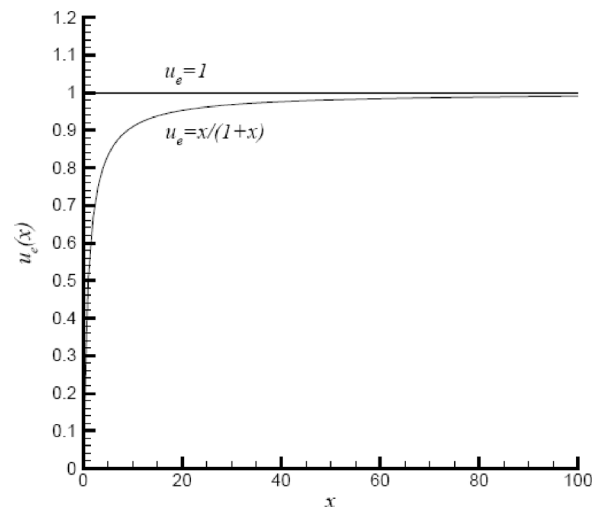

Fig. 6. External velocity profile.

The so-called boundary-layer thickness $\delta(x)$ is defined by

$$u(x, \delta(x)) = 0.99 u_e(x),$$

where u is the dimensionless velocity and u_e is the dimensionless external flow velocity, respectively. Substituting $u_e = \xi$ and $u = f_\eta$ into above equation, we have the algebraic equation

$$\left. \frac{\partial f(\xi, \eta)}{\partial \eta} \right|_{\eta = \delta(\xi)} = 0.99 \xi. \tag{38}$$

Alternatively, one can directly calculate the dimensional displacement thickness

$$\begin{aligned}
\bar{\delta} &= \int_0^{+\infty} \left[1 - \frac{\bar{u}(\bar{x}, \bar{y})}{\bar{u}_e(\bar{x})} \right] d\bar{y} \\
&= L_0 \left[\frac{\sigma(x)}{\mathrm{Re}^{14/2}} \right] \int_0^{+\infty} \left[1 - \frac{1}{u_e(x)} \frac{\partial f}{\partial \eta} \right] d\eta.
\end{aligned} \tag{39}$$

Defining the dimensionless displacement thickness $\delta^*(x) = \mathrm{Re}^{1/2} \bar{\delta}/L_0$ and using $u_e = \xi$, one has the dimensionless displacement thickness

$$\delta^*(x) = \sigma(x) \int_0^{+\infty} \left[1 - \frac{f_\eta(\xi, \eta)}{\xi} \right] d\eta \tag{40}$$

for the non-similarity flow.

As mentioned before, there are similarity boundary-layer flows when $u_e = 1$ and $u_e = x$, respectively. In case of $u_e = x$, the corresponding boundary-layer thickness and displacement thickness of the similarity ones are $\tilde{\delta}(x) = 2.3793$ and $\tilde{\delta}^*(x) = 0.6479$, respectively. In the case of $u_e = 1$, the corresponding boundary-layer thickness and displacement thickness are $\hat{\delta}(x) = 0.5\sqrt{x}$ and $\hat{\delta}^*(x) = 1.7208\sqrt{x}$, respectively. However, the expressions of the boundary-layer thickness $\delta(x)$ and the displacement thickness $\delta^*(x)$ of the non-similarity flow with $u_e = x/(1-x)$ are much more complicated. It is found that, for small x near $x = 0$, the boundary-layer thickness $\delta(x)$ is rather close to $\tilde{\delta}(x) = 2.3793$, as shown in Figure 7. However, for $x > 1$, the boundary-layer thickness $\delta(x)$ of the non-similarity flow is always less than $\hat{\delta}(x) = 5.0\sqrt{x}$ of the similarity ones with $u_e = 1$; for large x, $\delta(x)$ is closer to the similarity ones with $u_e = 1$. Therefore, with the external flow velocity u_e tends to 1 as $x \to +\infty$, the boundary-layer thickness $\delta(x)$ of the non-similarity flow tends to the boundary-layer thickness $\hat{\delta}(x) = 5.0\sqrt{x}$ of the similarity flow with $u_e = 1$. In other words, the influence
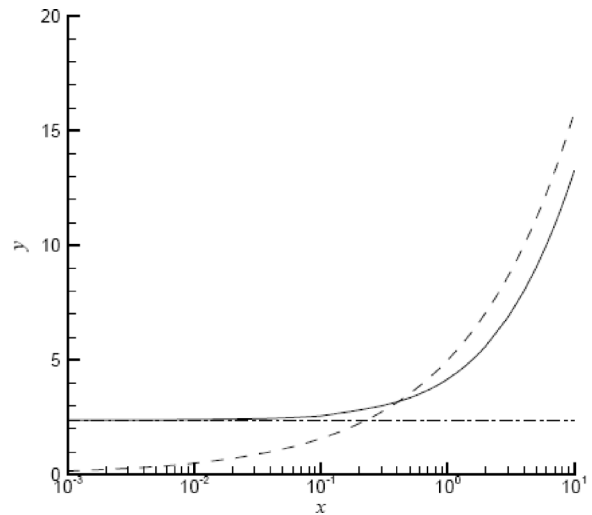

Fig. 7. Boundary-layer thickness near $x = 0$. Solid line: $\delta(x)$ for the non-similarity flow; Dash-dotted line: $\tilde{\delta}(x)$ for the similarity flow with $u_e = x$; Dashed line: $\hat{\delta}(x)$ for the similarity flow with $u_e = 1$.

of the non-similarity boundary-layer flow near $x \to +\infty$ fades away.

Similarly, it is found that near $x = 0$ the displacement thickness $\delta^*(x)$ of the non-similarity flow is rather close to $\tilde{\delta}^*(x) = 0.6479$ of the similarity flow with $u_e = x$, as shown in Figure 8. For large x, the displacement thickness $\delta^*(x)$ of the non-similarity flow is always less than $\tilde{\delta}^*(x) = 1.7208\sqrt{x}$ of the similar-
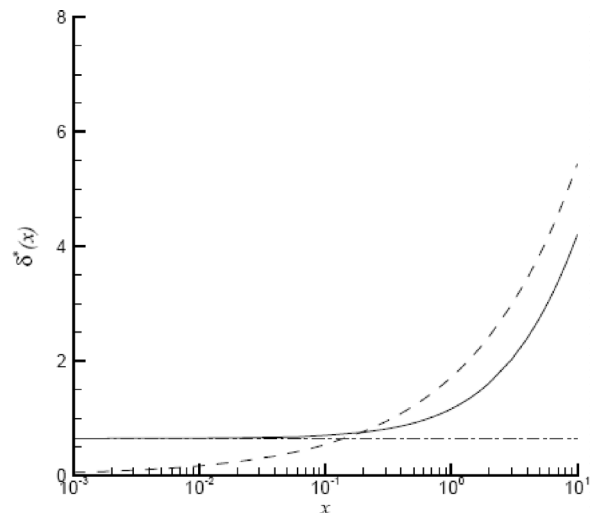

Fig. 8. Displacement thickness for small x; Solid line: $\delta^*(x)$ for the non-similarity flow; Dash-dotted line: $\tilde{\delta}^*(x)$ for the similarity flow with $u_e = x$; Dashed line: $\hat{\delta}^*(x)$ for the similarity flow with $u_e = 1$.
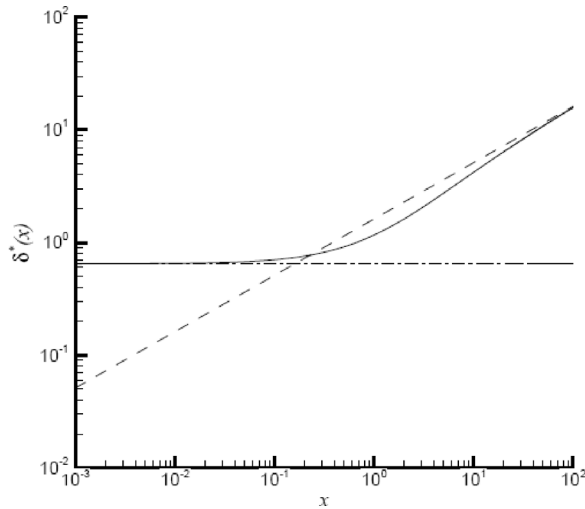
Fig. 9. Displacement thickness versus x; Solid line: the non-similarity flow; Dash-dotted line: $\delta^*(x) = 0.6479$ for the similarity flow with $u_e = x$; Dashed-line: $\hat{\delta}^*(x)$ for the similarity flow with $u_e = 1$.

ity flow with $u_e = 1$, as shown in Figure 9. Thus, for large x, the displacement thickness $\delta^*(x)$ of the non-similarity flow is always below the displacement thickness $\hat{\delta}^*(x)$ of the similarity ones with $u_e = 1$. This confirms the above conclusion that the influence of the non-similarity flow near $x \to +\infty$ dies away.

3.3. Skin Friction Coeffcient

The other significant physical quantity is the local skin friction coefficient

$$C_f(\bar{x}) = \frac{\tau_w(\bar{x})}{\frac{1}{2}\rho\bar{u}_e^2(\bar{x})} = \frac{2}{Re^{1/2}}\frac{\left.\frac{\partial^2 f}{\partial\eta^2}\right|_{\eta=0}}{\sigma(x)u_e^2(x)}$$

$$= \frac{2}{Re^{1/2}}\frac{(x+1)^{3/2}}{x^2}\left.\frac{\partial^2 f}{\partial\eta^2}\right|_{\eta=0}. \tag{41}$$

The dimensionless local skin friction coefficient is defined by

$$C_f(x) = C_f(\bar{x})Re^{1/2} = \frac{2(x+1)^{3/2}}{x^2}\left.\frac{\partial^2 f}{\partial\eta^2}\right|_{\eta=0}$$

$$= \frac{2\sqrt{1-\xi}}{\xi^2}\left.\frac{\partial^2 f}{\partial\eta^2}\right|_{\eta=0}. \tag{42}$$

By means of the homotopy analysis method, the accurate analytical approximation of $f_{\eta\eta}(\xi, 0)$ is ob-

tained, and the 30th-order approximation given by $\gamma = 4$ and $\hbar = -3/5$ reads

$$\begin{aligned}
f_{\eta\eta}(\xi, 0) = {}& 1.23259\xi - 0.547373\xi^2 \\
& - 0.125806\xi^3 - 0.0435865\xi^4 \\
& - 0.742626\xi^5 + 22.9772\xi^6 \\
& - 545.147\xi^7 + 9817.14\xi^8 \\
& - 138347\xi^9 + 1.55993 \times 10^6\xi^{10} \\
& - 1.4316 \times 10^7\xi^{11} + 1.08371 \times 10^8\xi^{12} \\
& - 6.83749 \times 10^8\xi^{13} + 3.62476 \times 10^9\xi^{14} \\
& - 1.62457 \times 10^{10}\xi^{15} + 6.18297 \times 10^{10}\xi^{16} \\
& - 2.00423 \times 10^{11}\xi^{17} + 5.54182 \times 10^{11}\xi^{18} \\
& - 1.30729 \times 10^{12}\xi^{19} + 2.62747 \times 10^{12}\xi^{20} \\
& - 4.48636 \times 10^{12}\xi^{21} + 6.47748 \times 10^{12}\xi^{22} \\
& - 7.85417 \times 10^{12}\xi^{23} + 7.9217 \times 10^{12}\xi^{24} \\
& - 6.55878 \times 10^{12}\xi^{25} + 4.37669 \times 10^{12}\xi^{26} \\
& - 2.29319 \times 10^{12}\xi^{27} + 9.07366 \times 10^{11}\xi^{28} \\
& - 2.54612 \times 10^{11}\xi^{29} + 4.51086 \times 10^{10}\xi^{30} \\
& - 3.78981 \times 10^9\xi^{31},
\end{aligned} \tag{43}$$

which agrees well with the 35th-order approximations and is accurate in the whole region $0 \le \xi \le 1$, i.e. $0 \le x < \infty$. Once the expression of $f_{\eta\eta}(\xi, 0)$ is obtained, the local coefficient of skin friction can be easily obtained.

As mentioned before, there exist similarity flows when $u_e = x$ and $u_e = 1$. In the case of $u_e = x$, the corresponding skin friction coefficient is given by $\tilde{C}_f = 2.46518/x$. In the case of $u_e = 1$, the skin friction coefficient is $\hat{C}_f = 0.66412/\sqrt{x}$. It is found that the skin friction coefficient $C_f(x)$ of the non-similarity flow is close to $\tilde{C}_f(x) = 2.46518/x$ near $x = 0$, as shown in Figure 10. This is reasonable, because, near $x = 0$, the corresponding boundary-layer thickness $\delta(x)$ and the displacement thickness $\delta^*(x)$ of the non-similarity flow also agree well with $\tilde{\delta}(x)$ and $\tilde{\delta}^*(x)$ of the similarity ones with the external flow velocity $u_e = x$, respectively. For large x, the skin coefficient $C_f(x)$ agrees well with $\hat{C}_f = 0.66412/\sqrt{x}$ for the similarity flow with $u_e = 1$, as shown in Figure 10. This is different from the boundary-layer thickness $\delta(x)$ and the displacement thickness $\delta^*(x)$ of the non-similarity flow, which have obvious differences from those of the similarity ones even as $x \to +\infty$. Note that the skin friction coefficient is related to $f_{\eta\eta}(\xi, 0)$, and thus is not affected
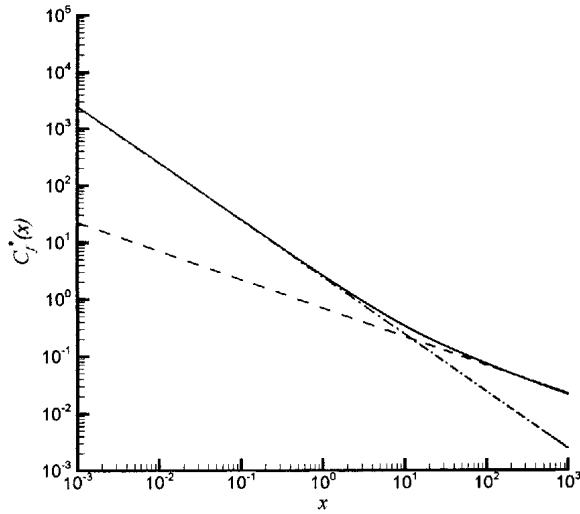
Fig. 10. Displacement thickness versus x; Solid line: the non-similarity flow; Dash-dotted line: $\tilde{C}_f(x) = 2.46518/x$ for the similarity flow with $u_e = x$; Dashed-line: $\hat{C}_f(x) = 0.66412/\sqrt{x}$ for the similarity flow with $u_e = 1$.

by the flow far from the plate. Besides, the boundary-layer thickness and the displacement thickness tend to infinity as $x \to +\infty$. Thus, even if the boundary-layer thickness $\delta(x)$ and the displacement thickness $\delta^*(x)$ of the non-similarity flow is different from those of the similarity ones, the skin friction coefficient of the non-similarity flow can be the same as that of the similarity ones with the external flow velocity $u_e = 1$ even as $x \to +\infty$. In other words, it is physically possible that the influence of the non-similarity flow on the skin friction coefficient dies away as $x \to +\infty$.

4. Conclusions and Discussions

In this paper, a kind of non-similarity boundary-layer flow of a Newtonian fluid near an asymmetric plane stagnation point with a dimensionless external flow velocity $u_e(x) = x/(x+1)$ is studied. The original boundary-layer equations are first transferred into a nonlinear PDE with variable coefficients. An analytic technique for strongly nonlinear problems, namely the homotopy analysis method (HAM), is then applied to replace the nonlinear PDE by an infinite number of linear ODEs with constant coefficients. An artificial parameter, called the convergence-control parameter, is introduced to ensure the convergence of series solution, and accurate analytic results are obtained.

Physically, it is interesting to compare the non-similarity flow of the variable external flow velocity

$u_e = x/(1 + x)$ with the similarity ones given by the uniform external flow velocity $u_e = 1$. It is found that, for $x > 1$, the boundary-layer thickness $\delta(x)$ of the non-similarity flow is always less than the boundary-layer thickness $\hat{\delta}(x)$ of the similarity ones. Similarly, for large x, the displacement thickness $\delta^*(x)$ of the non-similarity flow is always less than the displacement thickness $\hat{\delta}^*(x)$ of the similarity ones, too. It is rather interesting that, as $x \to +\infty$, the disturbance of the non-similarity boundary-layer flow near $x = 0$ does fade away even as $x \to +\infty$, where the external flow velocity becomes uniform. However, it is found that, as $x \to +\infty$, the local skin friction coefficient of the non-similarity flow tends to the same as that of the similarity ones. This is physically possible, because the skin friction coefficient is determined by the flow near the plate, and is not influenced by the far velocity field. So, as $x \to +\infty$, the skin friction coefficient of the non-similarity flow tends to be the same as that of the similarity ones.

Mathematically, it should be emphasized that the original nonlinear PDE (17) contains the derivatives with respect to both η and ξ, but the auxiliary linear operator (33) contains only derivatives with respect to η. In this way, the nonlinear PDE (17) with variable coefficients is transferred into an infinite number of linear ODEs with the constant coefficients. Obviously, it is much easier to solve an ODE than a PDE, especially by means of the symbolic computation software such as Mathematica, Maple, and so on. Why can we do in this way? This is mainly because, unlike all other analytic techniques, the HAM provides great freedom to choose the auxiliary linear operator, which is essentially the freedom on the choice of base functions. More importantly, unlike all other analytic techniques, the HAM introduces the so-called convergence-control parameter to ensure the convergence of the solution series, so that one *can* use this freedom to choose better base functions and the corresponding auxiliary linear operators: such kind of freedom has no meanings, if one can *not* ensure the convergence of solution series. It should be emphasized that the *same* auxiliary linear operator (33) has been applied to solve some similarity boundary-layer flows [29], which indicates that, by means of the HAM, the non-similarity flows can be solved in the same way as similarity ones!

Note that even the unsteady three-dimensional similarity boundary-layer flow due to a stretching surface in a rotating fluid is solved in a similar way: the coupled nonlinear PDEs are transferred into an infinite

number of decoupled, linear ODEs by means of the HAM with the auxiliary linear operators *independent* of the time [37]. Can all nonlinear PDEs be transferred into linear ODEs by means of the HAM? Note that, for boundary-layer flows, the velocity variation across the flow direction is much greater than that in the flow direction. This might be the physical reason why we can use the auxiliary linear operator (33) that is *independent* of ξ at all. This physical insight explains why the similarity and non-similarity boundary-layer flows can be solved by the same auxiliary linear operators (only related to η) in the framework of the HAM. It also reveals that many other types of non-similarity flows can be solved by the HAM in a similar way, and thus the proposed analytic approach has rather general meanings for boundary-layer flows. Furthermore, based on this physical insight, it should be impossible to replace a nonlinear PDE by an infinite number of linear ODEs, if the solution of the nonlinear PDE varies greatly in all directions. For example, the steady viscous flow around a sphere or a two-dimensional cylinder, governed by the exact Navier-Stokes equations, is much more complicated than boundary-layer flows, and thus might not be solved by the HAM in the similar way. A direct example supporting this view point is that the two-dimensional 2nd-order Gelfand equation is transferred into an infinite number of linear PDEs by means of the HAM using a 4th-order auxiliary partial differential operator, as shown by Liao and Tan [36]: this example once again illustrates the advantage of the HAM both on the freedom of choosing auxiliary linear operator and on the guarantee of convergence of solution series.

[1] K. Hiemenz, Dinglers J. **326**, 321 (1911).
[2] F. Homann, Z. Angew. Math. Mech. **16**, 153 (1936).
[3] J. Hadamard, Comptes Rendus **152**, 1735 (1911).
[4] L. Howarth, Philos. Mag. **42**, 1433 (1951).
[5] A. Davey, J. Fluid Mech. **10**, 593 (1960).
[6] C. Y. Wang, Q. Appl. Math. **32**, 207 (1974).
[7] B. S. Tilley and P. D. Weidman, Eur. J. Mech. B-Fluids **17**, 205 (1998).
[8] I. Pop, Z. Angew. Math. Mech. **63**, 580 (1983).
[9] P. S. Lawrence and B. N. Rao, J. Phys. D: Appl. Phys. **119**, 297 (2007).
[10] R. S. R. Gorla, Appl. Sci. Res. **32**, 541 (1976).
[11] W. H. H. Banks, J. Mec. Theor. Appl. **2**, 375 (1993).
[12] M. A. Chaudhary, J. H. Merkin, and I. Pop, Eur. J. Mech. B-Fluids **14**, 217 (1995).
[13] E. Magyari and B. Keller, Eur. J. Mech. B-Fluids **19**, 109 (2000).
[14] H. Schlichting and K. Gersten, Boundary Layer Theory, Springer, Berlin 2000.
[15] E. M. Sparrow and H. S. Quack, AIAA J. **8**, 1936 (1970).
[16] D. Catherall and W. Stewartson, Proc. R. Soc. A **14**, 481 (1962).
[17] E. M. Sparrow and H. S. Yu, J. Heat Transf. Trans. ASME **93**, 328 (1971).
[18] J. C. Hsieh, T. S. Chen, and B. F. Armaly, Int. J. Heat Mass Transf. **36**, 1485 (1993).
[19] M. Massoudi, Int. J. Non-Linear Mech. **36**, 961 (2001).
[20] Y. Y. Lok, N. Amin, and I. Pop, Z. Angew. Math. Mech. **83**, 594 (2003).
[21] N. Riley, SIAM Rev. **17**, 274 (1975).
[22] H. Xu and I. Pop, Acta Mech. **184**, 87 (2006).
[23] Y. Y. Lok, N. Amin, and I. Pop, Int. J. Therm. Sci. **45**, 1149 (2006).
[24] S. J. Liao, Commun. Nonlinear Sci. Numer. Simul. **14**, 2144 (2009).
[25] S. J. Liao, The proposed homotopy analysis technique for the solution of nonlinear problem, Ph.D. thesis, Shanghai Jiao Tong Univ. 1992.
[26] S. J. Liao, Beyond Perturbation: Introduction to the Homotopy Analysis Method, Chapman & Hall/CRC, Boca Raton 2003.
[27] S. J. Liao, Appl. Math. Comput. **147**, 499 (2004).
[28] S. J. Liao, Comm. Nonlinear Sci. Numer. Simul. **14**, 983 (2009).
[29] S. J. Liao, J. Fluid Mech. **385**, 101 (1999).
[30] S. J. Liao and E. Magyari, Z. Angew. Math. Phys. **57**, 777 (2006).
[31] S. Abbasbandy, Phys. Lett. A **360**, 109 (2006).
[32] S. P. Zhu, Quant. Financ. **6**, 229 (2006).
[33] M. Yamashita, K. Yabushita, and K. Tsuboi, J. Phys. A **40**, 8403 (2007).
[34] Y. Y. Wu and K. F. Cheung, Int. J. Numer. Meth. Fluids **57**, 1649 (2008).
[35] Y. Y. Wu and K. F. Cheung, Wave Motion **46**, 1 (2009).
[36] S. J. Liao and Y. Tan, Stud. Appl. Math. **119**, 297 (2007).
[37] Y. Tan and S. J. Liao, ASME J. Appl. Mech. **74**, 1011 (2007).

[38] L. Tao, H. Song, and S. Chakrabarti, Coast. Eng. **54**, 825 (2007).

[39] J. Cheng, J. Cang, and S. J. Liao, Z. Angew. Math. Phys. In Press, (2009).

[40] H. I. Andersson, Acta Math. **95**, 227 (1992).

[41] A. C. King, J. Billingham, and S. R. Otto, Differential Equations: Linear, Nonlinear Ordinary, Partial Cambridge U.P., Cambridge 2003.

[42] T. Cebeci and P. Bradshaw, Physical and computational aspects of convective heat transfer, Springer-Verlag, New York 1984.